Molecular Theory for Electrokinetic Transport in pH-Regulated Nanochannels

ARTICLE *in* JOURNAL OF PHYSICAL CHEMISTRY LETTERS · SEPTEMBER 2014

Impact Factor: 7.46 · DOI: 10.1021/jz5013802

5 AUTHORS, INCLUDING:

Xian Kong
Tsinghua University
11 PUBLICATIONS **9** CITATIONS
SEE PROFILE

Diannan Lu
Tsinghua University
78 PUBLICATIONS **865** CITATIONS
SEE PROFILE

Zheng Liu
Tsinghua University
137 PUBLICATIONS **1,731** CITATIONS
SEE PROFILE

Jianzhong Wu
University of California, Riverside
155 PUBLICATIONS **4,323** CITATIONS
SEE PROFILE

THE JOURNAL OF PHYSICAL CHEMISTRY Letters

Letter

pubs.acs.org/JPCL

Molecular Theory for Electrokinetic Transport in pH-Regulated Nanochannels

Xian Kong,[†,‡] Jian Jiang,[†] Diannan Lu,*[,‡] Zheng Liu,*[,‡] and Jianzhong Wu*[,†]

[†]Department of Chemical and Environmental Engineering and Department of Mathematics, University of California, Riverside, California 92521, United States

[‡]Department of Chemical Engineering, Tsinghua University, Beijing 100084, China

Supporting Information

ABSTRACT: Ion transport through nanochannels depends on various external driving forces as well as the structural and hydrodynamic inhomogeneity of the confined fluid inside of the pore. Conventional models of electrokinetic transport neglect the discrete nature of ionic species and electrostatic correlations important at the boundary and often lead to inconsistent predictions of the surface potential and the surface charge density. Here, we demonstrate that the electrokinetic phenomena can be successfully described by the classical density functional theory in conjunction with the Navier−Stokes equation for the fluid flow. The new theoretical procedure predicts ion conductivity in various pH-regulated nanochannels under different driving forces, in excellent agreement with experimental data.

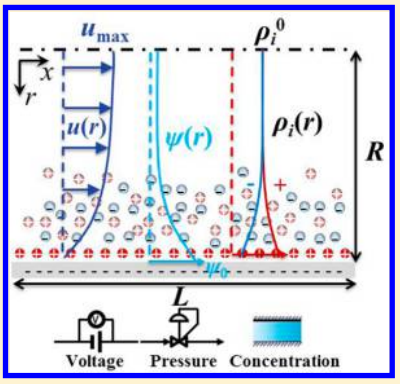

SECTION: Liquids; Chemical and Dynamical Processes in Solution

Recent advances in materials synthesis and nanofabrication enable the preparation of nanochannels with well-defined pore shape and surface chemistry, rending tremendous opportunities for new applications to nanofluidic systems.[1−5] Understanding electrokinetic transport through nanopores is important not only from fundamental perspectives[6−8] but also for the development of new electrochemical devices for DNA sequencing,[9,10] molecular level separation,[11−13] and energy harvesting from seawater.[14] A combination of strong confinement and surface influence makes ion transport in nanochannels drastically different from that corresponding to macroscopic systems.[15] However, existing theoretical models for interpretation of the experimental data for electrokinetic transport in nanopores are mostly based on continuous models that ignore the discrete nature of molecular species near the fluid−solid interface.[16−18] While the conventional methods work well when the surface charge density of a nanochannel is sufficiently low, the mean-field approach becomes problematic for describing ionic transport in highly charged nanopores. Recently, several modifications have been proposed[18] to fix the limitations of the conventional electrokinetic theory, including variation of the viscosity profile,[19,20] saturation of the electrophoretic mobility, inclusion of a low-dielectric layer at the surface,[17,18] and the slip length effects.[21,22] Usually, one needs to consider all of these modifications to reproduce experimental data for ionic flow in nanochannels,[18] which makes the theoretical procedure rather tedious. In this work, we present a new theoretical framework that alleviates some of the major limitations of conventional electrokinetic methods. The new method allows for a more faithful depiction of ion transport in nanopores under a broad range of experimental conditions, including those in nanochannels with large surface charge density that are particularly important for diverse nanofluidic applications such as energy harvesting and field effect transistors (FETs).[23−25]

Consider steady-state electrokinetic transport in a cylindrical pore of length L and radius R. As in typical experimental investigations of nanochannels, the pore size is on the nanoscale but much larger than the characteristic lengths of mobile ions and solvent molecules, and the pore length is macroscopic. Figure 1 shows schematically ion flow through the pore induced by one or multiple driving forces such as the gradients in electric potential ψ, pressure P, or bulk salt concentration ρ_s^0. In the presence of an external electric field, the electrical energy is converted to the kinetic energy for ion motion and the hydrodynamic energy of the solvent. Conversely, streaming current emerges when the ionic solution flows through a charged nanochannel driven by a pressure gradient,[8] which converts hydrodynamic energy to electrical energy. Similar energy conversion also holds when the bulk reservoirs at the ends of the nanochannel differ in salt concentration. In that case, the free-energy difference between two bulk solutions will be converted to electrical energy. The last two types of electrical currents have been under active

Received: July 2, 2014
Accepted: August 19, 2014
Published: August 19, 2014

   dx.doi.org/10.1021/jz5013802 | J. Phys. Chem. Lett. 2014, 5, 3015−3020

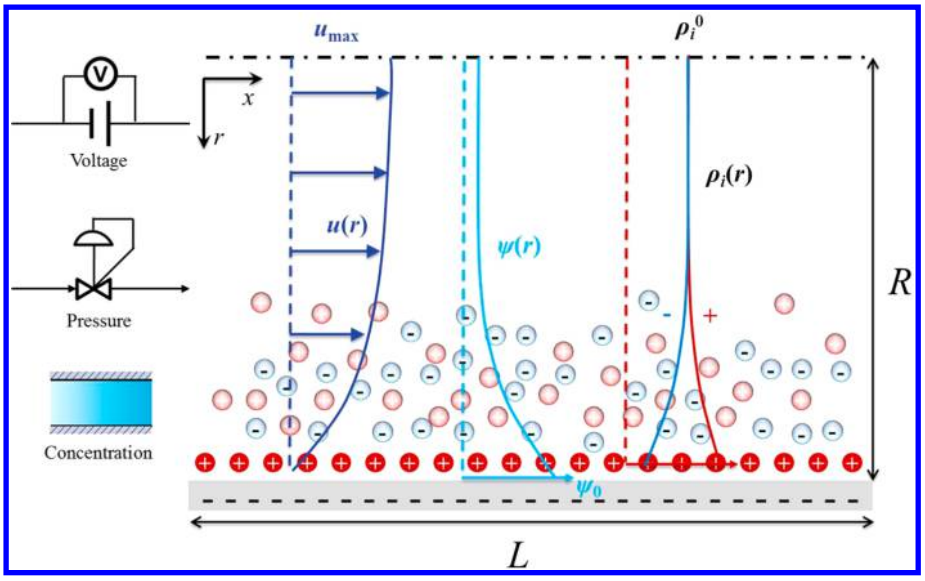

Figure 1. A schematic view of ion flow through a cylindrical pore of length L and radius R. The electrical current can be driven by three kinds of the external force, an electric field, a pressure gradient, or a concentration gradient.

investigations for renewable energy harvest. In all of these applications, a key quantity of practical concern is the electrical current, I, arising from the ion flow through the pore.

A theoretical description of the electrical current inside of the nanopore requires explicit models for the local chemical potentials of ionic species and their connections with the transport equations. Whereas the thermodynamic potential is conventionally expressed in terms of that from the ideal solution,[18,26] accurate theories are now available to quantify the local chemical potentials of inhomogeneous electrolyte solutions.[27] For electrokinetic transport of simple ions considered in this work, we use the primitive model, which represents the solvent as a dielectric continuum and the ions as charged hard spheres of equal size. As in numerous previous studies of bulk electrolyte solutions,[28] we take an ionic diameter of 0.4 nm for all hydrated monovalent ions, and the dielectric constant for water is $\varepsilon = 78.5$. The continuous description of the solvent is fully consistent with the electrokinetic equations for ion transport described below. While it provides no chemical details for the ionic species or solvent molecules, the primitive model is able to predict both the ionic distributions and thermodynamic properties of simple electrolytes even at high concentrations.[29,30] It has also been used extensively to study electrochemical properties including the microscopic details of the electric double layer (EDL).[31−33]

The electrical current is related to the axial component of the mean ion velocity $u_{x,i}(r,x)$ for each ionic species and the inhomogeneous ionic distributions inside of the pore $\rho_i(r,x)$[8]

$$I = 2\pi \int_0^R \sum_i Z_i e \rho_i(r, x) u_{x,i}(r, x) r \, dr \tag{1}$$

where e represents the unit charge and Z_i is the valence of ionic species i. Although the local potential and the local ionic density and velocity profiles generally vary in both axial (x) and radial (r) directions of the pore, the current density must be independent of the axial coordinate due to the conservation of mass at steady state.

The axial component of the mean ion velocity can be calculated from a superposition of the corresponding solvent velocity, $u_x(r,x)$, and ion motion due to the electrical field

$$u_{x,i}(r, x) = u_x(r, x) - eZ_i\upsilon_i\left[\frac{\partial\psi(r, x)}{\partial x}\right] \tag{2}$$

where $\psi(r,x)$ denotes the local electrical potential and υ_i represents the ion mobility. If the average ion concentration inside of the pore is moderate and the pore size is much larger than the length scale pertinent to the inhomogeneous distribution of solvent molecules near the pore surface, we may assume that the solvent is continuous and has uniform viscosity η throughout the pore. The continuous representation of the solvent is consistent with the thermodynamic model for the local chemical potentials of ionic species.

Application of the Navier−Stokes (NS) equation to the axial and radial directions of the solvent velocity, respectively, leads to

$$\frac{\eta}{r}\frac{\partial}{\partial r}\left[r\frac{\partial u_x(r, x)}{\partial r}\right] + \rho_e(r, x)\frac{\partial\psi(r, x)}{\partial x} + \frac{\partial P(r, x)}{\partial x} = 0 \tag{3}$$

$$\rho_e(r, x)\frac{\partial\psi(r, x)}{\partial r} + \frac{\partial P(r, x)}{\partial r} = 0 \tag{4}$$

where $P(r,x)$ represents the local pressure, and $\rho_e(r,x)$ denotes the local charge density. The latter is related to the local density of ionic species

$$\rho_e(r, x) = \sum_i Z_i e \rho_i(r, x) \tag{5}$$

Integration of eq 4 with respect to the radial coordinate gives

$$P(r, x) = P_0(x) - \int_0^r \rho_e(r, x)\frac{\partial\psi(r, x)}{\partial r} \, dr \tag{6}$$

where $P_0(x)$ is the pressure at the center of the cylindrical pore. The boundary condition for the solvent velocity is given by

$$\frac{du_x(r, x)}{dr} = \begin{cases} -u_x(R, x)/b & r = R \\ 0 & r = 0 \end{cases} \tag{7}$$

where b represents the solvent slip length.[8] A typical continuous model treats b as an empirical parameter depending

dx.doi.org/10.1021/jz5013802 | J. Phys. Chem. Lett. 2014, 5, 3015−3020

on the chemical details of the solvent−surface interactions. In general, the slip length is negative for water in contact with a hydrophilic surface and positive near a hydrophobic surface. For all systems considered in this work, the slip length has relatively small effects on the electric current, and we use $b = 0$ for all results discussed in the following.

To solve for the pressure and velocity profiles from the NS equation, we need a thermodynamic model to predict the ionic density profiles $\rho_i(r,x)$ and the local electrical potential $\psi(r,x)$. These two variables are explicitly related through the Poisson equation

$$\frac{1}{r}\frac{\partial}{\partial r}\left[r\frac{\partial \psi(r,x)}{\partial r}\right] + \frac{\partial^2 \psi(r,x)}{\partial x^2} = -\frac{e}{\varepsilon_0 \varepsilon}\sum_i Z_i \rho_i(r,x) \tag{8}$$

where ε_0 denotes the vacuum permittivity. The boundary conditions for $\psi(r,x)$ in the axial direction are specified by the electrical potentials at the two ends of the nanopore

$$\psi(0,x) = \begin{cases} 0 & x = 0 \\ \Delta\psi & x = L \end{cases} \tag{9}$$

and those in the radial direction are given by the conditions of axial symmetry and local charge neutrality, respectively

$$\left.\frac{\partial \psi(r,x)}{\partial r}\right|_{r=0} = 0 \tag{10}$$

$$Q(x) = -\frac{1}{R}\int_0^R \sum_i Z_i e \rho_i(r,x) r \, \mathrm{d}r \tag{11}$$

where $Q(x)$ represents the local surface charge density of the nanopore. Strictly speaking, charge neutrality is valid only when the axial length scale is macroscopic (as for systems considered in this work). For short pores, eq 11 must be replaced by the charge neutrality condition for the entire system.

The surface charge density of pH-regulated nanopores is determined by protonation and deprotonation equilibria of ionizable groups at the inner surface. Specifically, the solution pH affects the surface charge density of the nanochannel through the following titration reactions[16]

$$\mathrm{AH} \rightleftharpoons \mathrm{A^-} + \mathrm{H^+} \tag{12}$$

$$\mathrm{AH} + \mathrm{H^+} \rightleftharpoons \mathrm{AH_2^+} \tag{13}$$

where AH, $\mathrm{A^-}$, $\mathrm{AH_2^+}$ stand for neutral, deprotonated, and protonated chemical groups at the inner surface of the nanopore. After some straightforward algebra, we can derive the surface charge density in terms of the total density of the ionizable sites at the surface Γ_{total} and the surface electrical potential $\psi(R,x)$

$$Q(x) = e\Gamma_{\mathrm{total}}\left(\frac{K_\mathrm{P}\xi_0^2(x) - K_\mathrm{D}}{K_\mathrm{D} + \xi_0(x) + K_\mathrm{P}\xi_0^2(x)}\right) \tag{14}$$

where K_D and K_P are equilibrium constants for deprotonation (D) and protonation (P) reactions, respectively, $\xi_0(x) \equiv 10^{-\mathrm{pH}} \exp[-\beta e\psi(R,x)]$, and $\beta = 1/k_\mathrm{B}T$ is the inverse of the Boltzmann constant k_B and absolute temperature T.

If one follows the ideal solution model, the ionic density profiles and the electric potential would be connected through the Poisson−Boltzmann (PB) equation. While the classical approach remains popular in the literature, the ideal solution model is not justified for determining the inhomogeneous distributions of ionic species inside of the pore, and its performance is particularly problematic near a highly charged surface. To account for the thermodynamic nonideality and the surface potential beyond electrostatic and confining effects, we use instead the classical density functional theory (DFT) to calculate the ionic distributions[34]

$$\rho_i(r,x) = \rho_i^0 \exp[-\beta Z_i e\psi(r,x) - \beta\Delta\mu_i^{\mathrm{ex}}(r,x) - \beta \mathrm{X}_i(r,x)] \tag{15}$$

In eq 15, ρ_i^0 is the ion concentration of a bulk electrolyte at zero electrical potential, $\mu_i^{\mathrm{ex}}(r,x) \equiv \mu_i(r,x) - k_\mathrm{B}T\ln[\rho_i(r,x)\Lambda_i^3]$ is the local excess chemical potential of ion i, Λ_i is the thermal wavelength, $\Delta\mu_i^{\mathrm{ex}}(r,x)$ denotes the deviation of the local excess chemical potential from that in the bulk electrolyte, and $\mathrm{X}_i(r,x)$ accounts for the additional external potential due to specific interactions of ion i with the surface. The detailed expression for $\mu_i^{\mathrm{ex}}(r,x)$ can be found in Supporting Information. As documented in our previous publications,[35−39] the expression for $\mu_i^{\mathrm{ex}}(r,x)$ is quantitatively accurate in comparison with molecular simulation results. Without the excess chemical potential, eq 15 becomes identical to the conventional PB equation for ionic distributions.

While one may consider eq 15 as a generalized PB equation, the DFT method is formally exact; approximations are introduced only in the specific ion−surface interactions and in the excess chemical potential. In general, the external potential $\mathrm{X}_i(r,x)$ depends on the physiochemical details of the electrolyte and the nanopore at the atomic scale. While the exact form of the surface potential remains poorly understood, the specific interactions in liquid water are important only in the immediate vicinity of the surface, typically within a few layers of the solvent molecules.[17] By using hydration size parameters, the primitive model avoids the chemical details of ionic species and specific ion−surface interactions. In that case, $\mathrm{X}_i(r,x) = 0$, and the local excess chemical potential arises solely from ion-excluded volume effects and electrostatic correlations. Within this model, accurate density functionals have been developed to account for the thermodynamic nonideality of simple electrolyte solutions.[37,40−42]

For all systems considered in this work, we assert that the pore radius is much larger than the Debye screening length such that the electrical potential at the nanochannel center is not influenced by the EDL at the boundary. For numerical convenience, we assume further that $(\partial^2\psi(r,x))/\partial x^2 = 0$ at all radial positions, and the electrical potential, the local pressure, and the ideal chemical potential of each ion at the center of the nanopore are linear functions of the axial distance

$$\psi(0,x) = \psi(0,0) + \left(\frac{\Delta\psi}{L}\right)x \tag{16}$$

$$P(0,x) = P(0,0) + \left(\frac{\Delta P}{L}\right)x \tag{17}$$

$$\ln\frac{\rho_i(0,x)}{\rho_i(0,0)} = \frac{x}{L}\ln\frac{\rho_i(0,L)}{\rho_i(0,0)} \tag{18}$$

where $\Delta\psi$ and ΔP represent the voltage and pressure differences at the two ends of the pore, respectively.

Given a specific nanochannel, we will have the total number density of the ionizable sites at the surface Γ_{total} as well as the

dx.doi.org/10.1021/jz5013802 | J. Phys. Chem. Lett. 2014, 5, 3015−3020

equilibrium constants K_D and K_P according to the chemistry of the nanopore (viz. eq 12 and 13). From eqs 16−18, we can determine the pressure gradient, the electrical potential, and the ionic densities at the center of the nanopore based on the geometric parameters, R and L, the ion densities at the entrances, $\rho_i(0,0)$ and $\rho_i(0,L)$, and the differences in electrical potential and pressure, $\Delta\psi$ and ΔP, respectively. The ionic density profiles $\rho_i(r,x)$, the surface charge density, $Q(x)$, and the local electrical potential throughout the pore, $\psi(r,x)$, are then calculated from the simplified Poisson equation

$$\frac{1}{r}\frac{\partial}{\partial r}\left[r\frac{\partial\psi(r,x)}{\partial r}\right] = -\frac{e}{\varepsilon_0\varepsilon}\sum_i Z_i\rho_i(r,x) \tag{19}$$

and the DFT equation for the ionic density profiles

$$\rho_i(r,x) = \rho_i(0,x)\exp[-\beta Z_i e\psi(r,x) - \beta\Delta\mu_i^{ex}(r,x)] \tag{20}$$

Equations19 and 20 are solved iteratively in conjunction with the boundary conditions given by eqs 9−11 and the surface titration equilibrium, eq 14. The thermodynamic variables are then used as the input for solving the NS equation, eqs 3 and 4, from which the solvent as well as the ionic velocity profiles can be calculated. Finally, the electrical current can be calculated from eq 1 on the basis of the local ion density and velocity profiles together with the local electrical potential.

To calibrate the theoretical procedure discussed above, we compare its predictions with those from the conventional method and with the experimental data for ion transport through boron nitride nanotubes recently investigated by Bocquet and co-workers.[26] For convenience, we distinguish different theoretical procedures simply based on the thermodynamic model used for calculating the local ion densities and the excess chemical potentials. For boron nitride nanotubes, the number density of ionizable groups is $\Gamma_{total} = 18\ nm^{-2}$, and the protonation constants are $K_D = 10^{-5.5}$ and $K_P = 0$. The potassium and chlorine ions are assumed to have the same size, with a hydration diameter of 0.4 nm.

Figure 2a shows the dependence of conductance G on pH predicted by DFT and PB in comparison with experimental data.[26] Here, the electric conductance is calculated from the current I and the difference in electrical potential at the ends $\Delta\psi$

$$G = \frac{I}{\Delta\psi} \tag{21}$$

Both DFT and PB perform well at low pH when the nanochannel is moderately charged. At large pH, however, the surface charge density increases, and the PB equation drastically overpredicts the electric conductance. The discrepancy between DFT and PB at large pH is understandable because the EDL structure near a highly charged surface is sensitive to the ionic excluded volume effects and electrostatic correlations. Such effects are described faithfully by DFT but completely ignored in the PB equation, leading to artificially high salt concentration inside of the nanotube and unrealistic electric conductance. Apparently, the error is exacerbated when the PB calculation is coupled with the protonation equilibrium for determining the surface charge density. The poor performance of the PB equation for monovalent electrolyte solutions is consistent with previous reports of both DFT calculations[43,44] and MC simulations.[28]

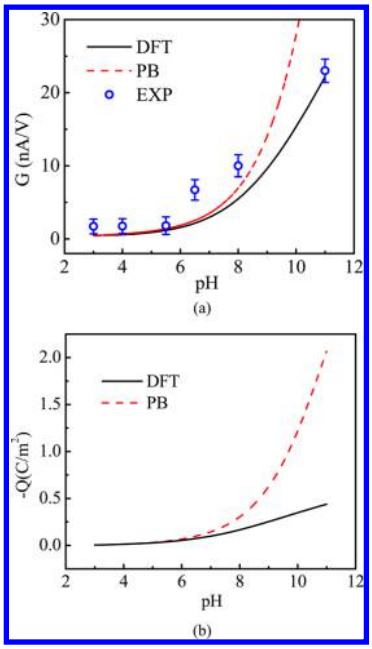

Figure 2. (a) Dependence of conductance G on pH predicted by DFT and PB in comparison with experimental data.[26] (b) Surface charge density Q versus pH predicted by DFT and PB. Here, the nanotube radius is R = 29 nm, and the length is L = 900 nm. The bulk concentration of salt (KCl) is 0.01M.

Figure 2b shows the corresponding surface charge density versus pH calculated from the PB and DFT equations, respectively. Here, the ion concentrations at the center of the nanopore are assumed invariant with the axial coordinate, and thus, the surface charge density is uniform throughout the pore. Again, the PB and DFT results are similar at low pH. When pH > 6.5, however, the PB equation predicts the surface charge density noticeably larger than that from the DFT calculations. For example, the surface charge density is about 1 C/m^2 at pH = 10 and 2 C/m^2 at pH = 11, but the corresponding results from DFT are 0.34 and 0.44 C/m^2, respectively.

Figure 3 compares the theoretical and experimental results for the streaming currents in a boron nitride nanotube of R = 29 nm and L = 900 nm at different pH values. Here, the pressure difference at the two ends of the nanotube is ΔP = 1 bar, and the bulk salt concentration is 0.01 M. We see that the PB equation fails to reproduce the experimental data at high pH, while DFT captures the behavior almost quantitatively.

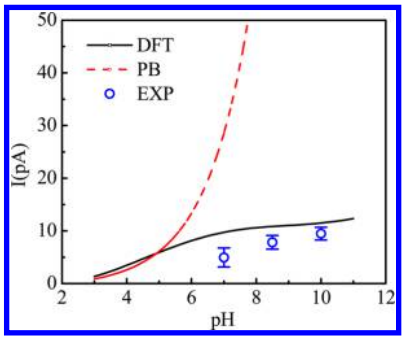

Figure 3. Dependence of streaming current on pH predicted by DFT and PB in comparison with experimental data.[26] Here, the nanotube radius is R = 29 nm, and the length is L = 900 nm. The bulk concentration of salt is 0.01M.

dx.doi.org/10.1021/jz5013802 | J. Phys. Chem. Lett. 2014, 5, 3015−3020

Again, the DFT and PB equations yield similar results at low pH or when the surface charge density is not too large. At large pH, the PB equation predicts that the streaming current increases almost exponentially with the pH, while the DFT predicts an asymptotic behavior in good agreement with experiment. In stark contrast to the PB equation, the DFT performs better with increasing pH. As the surface charge density increases, the effects of ion size and charge correlation effects become more predominant in comparison to nonspecific ion−surface interactions. We expect that the latter is important at low pH when the surface charge density is small. In that case, the nonelectrostatic effects, such as low dielectric layer near the channel surface may also affect the transport behavior. Because the primitive model ignores the molecular-level details, the discrepancy between DFT and experimental results is expected to be more significant for ion transport in nanotubes of low surface charge density.

We find that the new theoretical procedure works equally well for electrokinetic flow induced by the concentration gradient inside of the pore. Figure 4 shows theoretical predictions from both DFT and PB in comparison with the experimental measurements for the electric current induced by concentration differences at the two ends of a nanotube of 40 nm in radius and 1250 nm in length. Similar to previous situations, at lower pH, both DFT and PB could give satisfactory predictions, but at high pH values, the PB theory predicts an erroneous rapid increase of the currents. By contrast, the DFT performs well at all pH values.

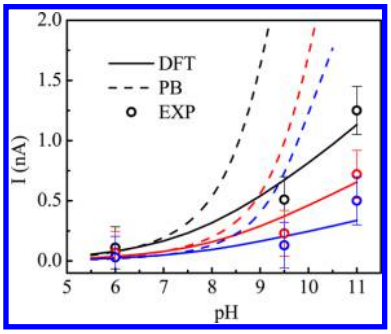

Figure 4. Dependence of osmotic current on pH predicted by DFT and PB in comparison with experimental data.[26] Here, the nanotube radius is R = 40 nm, and the length is L = 1250 nm.

To conclude, we have shown that replacing the PB equation with the classical DFT eliminates some major limitations of the conventional electrokinetic theory for describing ion transport in nanochannels. The new theoretical procedure successfully accounts for molecular excluded volume effects and electrostatic correlations that are important for ion transport in highly charged nanopores. In conjunction with the standard hydrodynamic equations and chemical equilibrium thermodynamics for surface ionization, the DFT-based procedure predicts electrical currents induced by different driven forces in excellent agreement with experimental data. By contrast, the conventional theory severely overpredicts the current and surface charge density for ion flow in highly charged nanochannels and requires different sets of surface charge densities for different driving forces.[18,26]

■ ASSOCIATED CONTENT

Supporting Information

Simplified equations for specific cases, computational details for solving the ionic distributions and deprotonation equilibrium, and precise expressions for the local excess chemical potentials in the DFT calculation. This material is available free of charge via the Internet at http://pubs.acs.org.

■ AUTHOR INFORMATION

Corresponding Authors

*E-mail: jwu@engr.ucr.edu (J.W.).
*E-mail: ludiannan@tsinghua.edu.cn (D.L.).
*E-mail: liuzheng@mail.tsinghua.edu.cn (Z.L.).

Notes

The authors declare no competing financial interest.

■ ACKNOWLEDGMENTS

K.X. is grateful to the Chinese Scholarship Council for the visiting fellowship. This work was supported as part of the Fluid Interface Reactions, Structures and Transport (FIRST) Center, an Energy Frontier Research Center funded by the U.S. Department of Energy, Office of Science, Office of Basic Energy Sciences. Additional support is provided by National Natural Science foundation of China, No. 21276138, and Tsinghua University Foundation, No. 2013108930. The numerical calculations were performed at the National Energy Research Scientific Computing Center (NERSC).

■ REFERENCES

(1) Napoli, M.; Eijkel, J. C. T.; Pennathur, S. Nanofluidic technology for biomolecule applications: a critical review. *Lab Chip* **2010**, *10*, 957−985.
(2) Wang, Q. H.; Bellisario, D. O.; Drahushuk, L. W.; Jain, R. M.; Kruss, S.; Landry, M. P.; Mahajan, S. G.; Shimizu, S. F. E.; Ulissi, Z. W.; Strano, M. S. Low dimensional carbon materials for applications in mass and energy transport. *Chem. Mater.* **2014**, *26*, 172−183.
(3) van der Heyden, F. H. J.; Stein, D.; Dekker, C. Streaming currents in a single nanofluidic channel. *Phys. Rev. Lett.* **2005**, *95*, 116104.
(4) van der Heyden, F. H. J.; Bonthuis, D. J.; Stein, D.; Meyer, C.; Dekker, C. Power generation by pressure-driven transport of ions in nanofluidic channels. *Nano Lett.* **2007**, *7*, 1022−1025.
(5) Stein, D.; Kruithof, M.; Dekker, C. Surface-charge-governed ion transport in nanofluidic channels. *Phys. Rev. Lett.* **2004**, *93*, 035901.
(6) Sparreboom, W.; van den Berg, A.; Eijkel, J. C. T. Principles and applications of nanofluidic transport. *Nat. Nanotechnol* **2009**, *4*, 713−720.
(7) Schoch, R. B.; Han, J. Y.; Renaud, P. Transport phenomena in nanofluidics. *Rev. Mod. Phys.* **2008**, *80*, 839−883.
(8) Bocquet, L.; Charlaix, E. Nanofluidics, from bulk to interfaces. *Chem. Soc. Rev.* **2010**, *39*, 1073−1095.
(9) Liu, H. T.; He, J.; Tang, J. Y.; Liu, H.; Pang, P.; Cao, D.; Krstic, P.; Joseph, S.; Lindsay, S.; Nuckolls, C. Translocation of single-stranded DNA through single-walled carbon nanotubes. *Science* **2010**, *327*, 64−67.
(10) Li, J.; Gershow, M.; Stein, D.; Brandin, E.; Golovchenko, J. A. DNA molecules and configurations in a solid-state nanopore microscope. *Nat. Mater.* **2003**, *2*, 611−615.
(11) Joshi, R. K.; Carbone, P.; Wang, F. C.; Kravets, V. G.; Su, Y.; Grigorieva, I. V.; Wu, H. A.; Geim, A. K.; Nair, R. R. Precise and ultrafast molecular sieving through graphene oxide membranes. *Science* **2014**, *343*, 752−754.
(12) Lee, C. Y.; Choi, W.; Han, J. H.; Strano, M. S. Coherence resonance in a single-walled carbon nanotube ion channel. *Science* **2010**, *329*, 1320−1324.

(13) Gillespie, D.; Pennathur, S. Separation of ions in nanofluidic channels with combined pressure-driven and electro-osmotic flow. *Anal. Chem.* **2013**, *85*, 2991−2998.
(14) Daiguji, H.; Yang, P. D.; Szeri, A. J.; Majumdar, A. Electrochemomechanical energy conversion in nanofluidic channels. *Nano Lett.* **2004**, *4*, 2315−2321.
(15) Duan, C. H.; Majumdar, A. Anomalous ion transport in 2-nm hydrophilic nanochannels. *Nat. Nanotechnol.* **2010**, *5*, 848−852.
(16) Yeh, L. H.; Zhang, M. K.; Qian, S. Z. Ion transport in a pH-regulated nanopore. *Anal. Chem.* **2013**, *85*, 7527−7534.
(17) Bonthuis, D. J.; Gekle, S.; Netz, R. R. Dielectric profile of interfacial water and its effect on double-layer capacitance. *Phys. Rev. Lett.* **2011**, *107*, 166102.
(18) Bonthuis, D. J.; Netz, R. R. Unraveling the combined effects of dielectric and viscosity profiles on surface capacitance, electro-osmotic mobility, and electric surface conductivity. *Langmuir* **2012**, *28*, 16049−16059.
(19) Lyklema, J. On the slip process in electrokinetics. *Colloids Surf., A* **1994**, *92*, 41−49.
(20) Wu, P.; Qiao, R. Physical origins of apparently enhanced viscosity of interfacial fluids in electrokinetic transport. *Phys. Fluids* **2011**, *23*, 072005.
(21) Heinbuch, U.; Fischer, J. Liquid flow in pores — slip, no-slip, or multilayer sticking. *Phys. Rev. A* **1989**, *40*, 1144−1146.
(22) Joly, L.; Ybert, C.; Trizac, E.; Bocquet, L. Liquid friction on charged surfaces: from hydrodynamic slippage to electrokinetics. *J. Chem. Phys.* **2006**, *125*, 204716.
(23) Karnik, R.; Fan, R.; Yue, M.; Li, D. Y.; Yang, P. D.; Majumdar, A. Electrostatic control of ions and molecules in nanofluidic transistors. *Nano Lett.* **2005**, *5*, 943−948.
(24) Paik, K. H.; Liu, Y.; Tabard-Cossa, V.; Waugh, M. J.; Huber, D. E.; Provine, J.; Howe, R. T.; Dutton, R. W.; Davis, R. W. Control of DNA capture by nanofluidic transistors. *ACS Nano* **2012**, *6*, 6767−6775.
(25) Guan, W. H.; Fan, R.; Reed, M. A. Field-effect reconfigurable nanofluidic ionic diodes. *Nat. Commun.* **2011**, *2*, 506.
(26) Siria, A.; Poncharal, P.; Biance, A. L.; Fulcrand, R.; Blase, X.; Purcell, S. T.; Bocquet, L. Giant osmotic energy conversion measured in a single transmembrane boron nitride nanotube. *Nature* **2013**, *494*, 455−458.
(27) Kunz, W. *Specific Ion Effects*; World Scientific: Singapore; Hackensack, NJ, 2010.
(28) Ibarra-Armenta, J. G.; Martin-Molina, A.; Quesada-Perez, M. Influence of monovalent ion size on colloidal forces probed by Monte Carlo simulations. *Phys. Chem. Chem. Phys.* **2011**, *13*, 13349−13357.
(29) Simonin, J. P.; Blum, L.; Turq, P. Real ionic solutions in the mean spherical approximation. 1. Simple salts in the primitive model. *J. Phys. Chem.* **1996**, *100*, 7704−7709.
(30) Burgess, J. *Ions in Solution: Basic Principles of Chemical Interactions*; E. Horwood; Halsted Press: Chichester, England; New York, 1988.
(31) Wu, J.; Jiang, T.; Jiang, D.-e.; Jin, Z.; Henderson, D. A classical density functional theory for interfacial layering of ionic liquids. *Soft Matter* **2011**, *7*, 11222−11231.
(32) Jiang, D. E.; Jin, Z. H.; Wu, J. Z. Oscillation of capacitance inside nanopores. *Nano Lett.* **2011**, *11*, 5373−5377.
(33) Jiang, D. E.; Wu, J. Z. Microscopic insights into the electrochemical behavior of nonaqueous electrolytes in electric double-layer capacitors. *J. Phys. Chem. Lett.* **2013**, *4*, 1260−1267.
(34) Wu, J. Z.; Li, Z. D. Density-functional theory for complex fluids. *Annu. Rev. Phys. Chem.* **2007**, *58*, 85−112.
(35) Jiang, J.; Cao, D. P.; Henderson, D.; Wu, J. Z. Revisiting density functionals for the primitive model of electric double layers. *J. Chem. Phys.* **2014**, *140*, 044714.
(36) Jiang, J.; Cao, D. P.; Henderson, D.; Wu, J. Z. A contact-corrected density functional theory for electrolytes at an interface. *Phys. Chem. Chem. Phys.* **2014**, *16*, 3934−3938.
(37) Li, Z.; Wu, J. Density functional theory for polyelectrolytes near oppositely charged surfaces. *Phys. Rev. Lett.* **2006**, *96*, 048302.
(38) Li, Z. D.; Wu, J. Z. Density functional theory for planar electric double layers: Closing the gap between simple and polyelectrolytes. *J. Phys. Chem. B* **2006**, *110*, 7473−7484.
(39) Wu, J. Z.; Jiang, T.; Jiang, D. E.; Jin, Z. H.; Henderson, D. A classical density functional theory for interfacial layering of ionic liquids. *Soft Matter* **2011**, *7*, 11222−11231.
(40) Yu, Y. X.; Wu, J. Z. Structures of hard-sphere fluids from a modified fundamental-measure theory. *J. Chem. Phys.* **2002**, *117*, 10156−10164.
(41) Li, Z.; Wu, J. Density-functional theory for the structures and thermodynamic properties of highly asymmetric electrolyte and neutral component mixtures. *Phys. Rev. E* **2004**, *70*, 031109.
(42) Li, Z.; Wu, J. Density functional theory for planar electric double layers: closing the gap between simple and polyelectrolytes. *J. Phys. Chem. B* **2006**, *110*, 7473−7484.
(43) Mier-y-Teran, L.; Suh, S. H.; White, H. S.; Davis, H. T. A nonlocal free-energy density-functional approximation for the electrical double-layer. *J. Chem. Phys.* **1990**, *92*, 5087−5098.
(44) Yu, Y. X.; Wu, J. Z.; Gao, G. H. Density-functional theory of spherical electric double layers and zeta potentials of colloidal particles in restricted-primitive-model electrolyte solutions. *J. Chem. Phys.* **2004**, *120*, 7223−7233.